Journal of Marine Science and Technology

Volume 22 | Issue 2 Article 9

HYDRODYNAMIC STUDY OF A FIXED PONTOON STRUCTURE UNDER WAVE LOADS WITH DIFFERENT REYNOLDS NUMBERS

Parviz Ghadimi
Department of Marine Technology, Amirkabir University of Technology, Tehran, Iran., pghadimi@aut.ac.ir

Farzam Safarzadeh Maleki
Department of Marine Technology, Amirkabir University of Technology, Tehran, Iran.

Mohammad A. Feizi Chekab
Department of Marine Technology, Amirkabir University of Technology, Tehran, Iran.

Journal of Marine Science and Technology, Vol. 22, No. 2, pp. 186-195 (2014)
DOI: 10.6119/JMST-013-0311-2

HYDRODYNAMIC STUDY OF A FIXED PONTOON STRUCTURE UNDER WAVE LOADS WITH DIFFERENT REYNOLDS NUMBERS

Parviz Ghadimi, Farzam Safarzadeh Maleki, and Mohammad A. Feizi Chekab

Key words: finite volume method, volume of fluid method, suspended fixed pontoons, hydrodynamic coefficients, regular waves, transmission coefficient.

ABSTRACT

As a breakwater, a suspended fixed pontoon is expected to receive energy of the wave and to reduce the wave height at downstream as much as possible. However, in other applications like floating bridges, the structure is expected to allow the wave to pass with the lowest possible energy absorption. In the present study, a numerical investigation has been conducted to identify the effective types of floating pontoon with different rectangular and circular cross sections under regular waves at different Reynolds numbers. Volume of fluid scheme and finite volume methods have been applied for tracking the free surface and discretization of the governing equations, respectively. To implement these numerical schemes, a computer code was developed and validated, which computes the lift and drag as well as the transmission coefficient for each of the moored fixed structures.

I. INTRODUCTION

Interaction of wave motion and fixed suspended systems can be cited as one example where the accurate modeling of waves can be very instrumental in the appropriate design of such systems. Fixed floating systems have vast areas of applications including the moored floating production platforms in deep waters or floating docks in shallow waters. Fixed suspended rigid body such as breakwater can be considered as one of these systems which are mainly used as wave attenuator at minor harbors and to some extent minor ports where the tranquility requirement is low. It is also used in places where the marine soil characteristics do not permit the installation of submerged or any other type of breakwater which require a good foundation. Due to these reasons, moored floating breakwater has been an important area of coastal and harbor research. Accordingly, all of the influential factors such as pontoon structures, wave forces and their interactions must carefully be studied and taken into consideration, when designing the structure and its mooring system. This paper does precisely that. It investigates the effect of the pontoon geometry and the effect of changes in Reynolds numbers proportion to hydrodynamic coefficients, calculates the wave forces and profiles and determines the lift and drag forces as well as the transmission coefficient involved.

Several studies dealing with the hydrodynamic problem of fixed and free bodies have been reported. Linear models and analytical solutions, which describe the full hydrodynamic problem, have been developed by Hwang and Tang (1986) [10], Williams and McDougal (1991) [24], Bhatta and Rahman (1993) [2], Isaacson and Bhat (1998) [11], Williams *et al*. (2000) [26] and Kriezi *et al*. (2001) [13]. As offshore oil and gas drilling and production activities have been pushed into deeper and deeper waters [27], the investigation of fixed floating breakwaters has become imperative and has attracted huge attention. During the past two decades, many types of fixed and floating breakwaters have been introduced and put in practice. McCartney (1985) [18] introduced four types of floating breakwaters including the box, pontoon, mat, and tethered, and analyzed their advantages and disadvantages. Mani (1991) [17] determined the transmission coefficients of the pontoon, mat, and tethered breakwaters, and Drimer *et al*. (1992) [8] offered a simplified design for a floating breakwater in which the breakwater width and the incident wavelength were much larger than the gap between the breakwater and the sea bed.

On the other hand, Murani and Mani (1997) [19] measured the transmission coefficients of a cage floating breakwater under wave and wave-current conditions. Sannasiraj *et al*. (1997) [20] conducted an experimental and theoretical investigation of behavior of pontoon-type floating breakwaters and studied the motion responses, the mooring forces, and the wave attenuation characteristics. Williams and Abul-Azm (1997) [25] studied the hydrodynamic properties of a dual pontoon floating breakwater consisting of a pair of rectangular

Paper submitted 06/30/11; revised 09/11/12; accepted 03/11/13. Author for correspondence: Parviz Ghadimi (e-mail: pghadimi@aut.ac.ir).
Department of Marine Technology, Amirkabir University of Technology, Tehran, Iran.

sectional floating cylinders connected by a rigid deck, while Bayram (2000) [1] conducted an experimental study of an inclined pontoon breakwater in intermediate water depths for use with small commercial vessels and yacht marinas. Williams *et al*. (2000) [26] theoretically investigated the hydrodynamic properties of a pair of long floating rectangular pontoon breakwaters and Liang *et al*. (2004) [14] proposed the spar buoy floating breakwater and determined the wave transmission characteristic and the wave induced tension of the mooring lines. Jung *et al*. (2004) [12] in their research titled as "Two-dimensional flow characteristics of wave interactions with a fixed rectangular structure" investigated the wave interactions on a fixed rectangular structure to simulate the condition of a barge in a beam sea. Consequently, several numerical models were developed to investigate the flow around submerged or floating structures. Milne-Thomson's circle theorem was used to study the characteristics of a two-dimensional irrotational flow around a horizontal cylinder under long-crested waves by Chaplin (1981) [5], while the discrete vortex method was employed by Sarpkaya (1989) [21]. Braza *et al*. (1986) [4] presented numerical simulations on the flow field at the near wake of a circular cylinder based on a finite volume velocity-pressure formulation of the unsteady Navier-Stokes equations. A Navier-Stokes time-stepping model was employed to compute the orbital flow motion around a circular cylinder by Chaplin (1993) [6].

For simulating the water waves, many different approaches have been presented. Mader (2004) [16] in his book has introduced several methods for numerical modeling of water waves. Tseng (2010) [22] has offered an efficient finite-difference implicit MacCormack scheme for simulation of one-dimensional kinematic wave flows. Lin (2010) [15] has reviewed several different numerical methods for modeling the water waves.

In the present study, hydrodynamic interaction of various regular waves with fixed rigid pontoons at different Reynolds numbers are evaluated in two dimensions. Influence of the incident wave characteristics and certain geometric characteristics such as width, height and diameter of the pontoon structure on its efficiency is examined. The considered structures include four different pontoon configurations as follows:

(a) circular cross section cylinder with diameter D = H = 3 m.
(b) H*W quadrilateral cross section cylinder W = H/3 = 1 m.
(c) H*2W quadrilateral cross section cylinder.
(d) H*3W quadrilateral cross section cylinder which happens to be of H*H size.

II. THEORETICAL FORMULATIONS

In this section, formulation and assumptions of the governing equations for the problem are summarized. The governing equations are derived from the incompressible Navier-Stokes equations and the continuity equation in the Cartesian coordinates system (x, y) given as

$$\rho\left[\frac{\partial v_x}{\partial t}+v_x\frac{\partial v_x}{\partial x}+v_y\frac{\partial v_x}{\partial y}\right]=-\frac{\partial P}{\partial x}+\mu\left[\frac{\partial^2 v_x}{\partial x^2}+\frac{\partial^2 v_x}{\partial y^2}\right]$$
$$\rho\left[\frac{\partial v_y}{\partial t}+v_x\frac{\partial v_y}{\partial x}+v_y\frac{\partial v_y}{\partial y}\right]=-\rho g\vec{k}-\frac{\partial P}{\partial y}+\mu\left[\frac{\partial^2 v_y}{\partial x^2}+\frac{\partial^2 v_y}{\partial y^2}\right] \quad (1)$$

$$\nabla\bullet\vec{v}=\frac{\partial v_x}{\partial x}+\frac{\partial v_y}{\partial y}=0 \quad (2)$$

where (v_x, v_y) is flow velocity in x and y directions; t is the time, ρ is the water density; p is the pressure; g is the gravitational acceleration; and υ is the kinematic viscosity coefficient. These equations totally explain the required parameters in any fluid field.

In order to simulate the free surface, Volume of Fluid (VOF) method is used. The basis of VOF method applied in this paper is the fractional volume of fluid scheme for tracking free boundaries. In this technique, a function $F(x, y, t)$ is defined whose value is unity at any point occupied by fluid and zero elsewhere. When averaged over the cells of a computational mesh, the average value of F in a cell is equal to the fractional volume of the cell occupied by the fluid. In particular, a unit value of F corresponds to a cell full of fluid, whereas a zero value indicates that the cell contains no fluid. Cells with F values between zero and one contain a free surface. The VOF method requires only one storage word for each mesh cell, which is consistent with the storage requirements for all other dependent variables. In addition to defining which cells contain a boundary, the F function can be used to define where the fluid is located in a boundary cell. Normal direction to the boundary lies in the direction in which the value of F changes most rapidly. When F is properly computed, the derivatives can then be used to determine the direction of normal to the boundary. Finally, when the normal direction and the value of F in a boundary cell are known, a line cutting the cell can be constructed that approximates the interface there. Additionally, surface curvatures can be computed for the definition of surface tension forces. The time dependence of F is governed by the equation

$$\frac{\partial F}{\partial t}+u\frac{\partial F}{\partial x}+v\frac{\partial F}{\partial y}=0, \quad (3)$$

where (u, v) are the fluid velocities in the coordinate directions (x, y). This equation is called "volume of fluid transport equation" and states that F moves with the fluid. These two sets of equations are solved by applying finite volume method. Accordingly, discretization of the 2D domain is the first step. Fig. 1 shows the unknown positions in a computational mesh. As evidenced in the figure, velocities are calculated at the middle of each face of the quadrilateral element, while pressure and F parameters are measured at the center of the element.

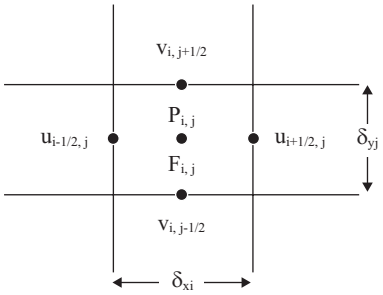

Fig. 1. Node position in a cell. (F is volume fraction, P is pressure, u and v are velocity components and i and j are cell indices in horizontal and vertical directions, respectively.)

Basic procedure for advancing a solution through one increment in time, δt, consists of three steps which are briefly outlined as follows:

(1) Explicit approximations of Eq. (1) are used to compute the first guess for the new time-level velocities using the initial conditions or previous time-level values for all advective, pressure, and viscous accelerations.
(2) To satisfy the continuity equation, i.e. Eq. (2), pressures are iteratively adjusted in each cell and the velocity changes induced by each pressure change are added to the velocities computed in step (l). Here, an iteration is required, because the change in pressure needed in one cell to satisfy Eq. (2), will upset the balance in the four adjacent cells.
(3) Finally, the *F* function defining fluid regions must be updated to give the new fluid configuration.

Repetition of these steps will advance a solution through any desired time interval.

III. NUMERICAL VALIDATION

The proposed code has been tested on two well-known validation problems; driven cavity flow and dam break problem.

1. Driven Cavity Flow

The flow in a closed cavity, driven by the motion of one wall across the cavity, has been extensively studied for many years. A comprehensive study illustrates the complexity of the flows which is involved in numerical solutions of the problem. Results for one driven cavity problem, i.e. a square cavity, in the form of vertical velocity with the Reynolds Numbers of 100, 1000, 5000 and 10000 are presented in Fig. 2 as a demonstration problem.

As observed in Fig. 2, the present results are in complete agreement with earlier numerical findings which indicates the effectiveness of the current code.

2. Dam Break

The classical problem of Dam Break [3, 23] has also been used for validation of the current free surface modeling. The

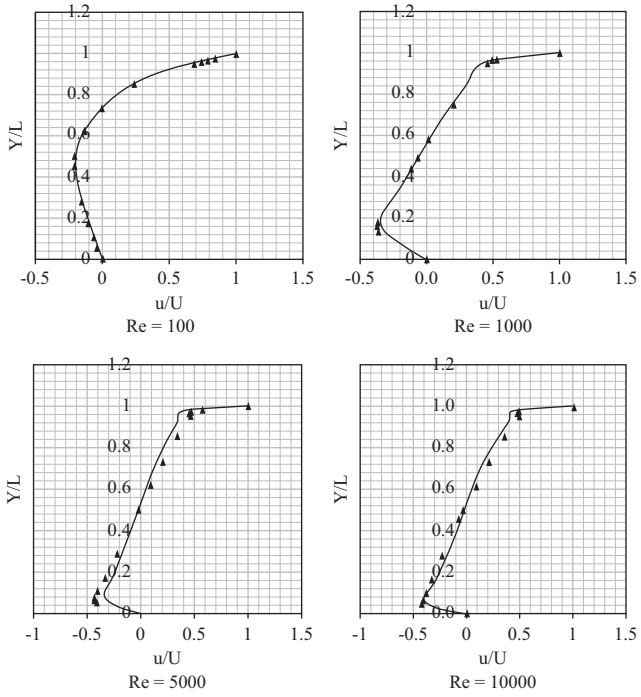

Fig. 2. Velocity in driven cavity; Ghia *et al*. (1982) [9]: triangle symbol (▲); Present work: solid line (—). (u is the horizontal velocity, U is the applied tangential velocity on the cavity, Y is the vertical coordinate and L is the total height of the cavity.)

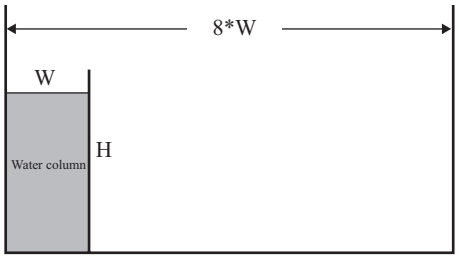

Fig. 3. Geometry of the Dam Break problem. (H and W are the height and width of the water column, respectively.)

test case refers to a water column which is suddenly allowed to collapse into a rectangular tank (Fig. 3).

The experimental data [23] reported for this test case contains the leading edge position of the collapsing column and the maximum height versus time. Results of the current numerical model, compared to the measurements in Figs. 4 and 5, show quite good agreement, especially when referring to the decrease of the maximum height of the column.

IV. PROBLEM DEFINITION AND METHODOLOGY

The concept of wave interaction with the pontoon structures constitutes a multidisciplinary problem where a combination of fluid mechanics as well as fluid dynamic and dynamic behavior of mechanical systems are introduced to perform a complete analysis capable of identifying the interactions

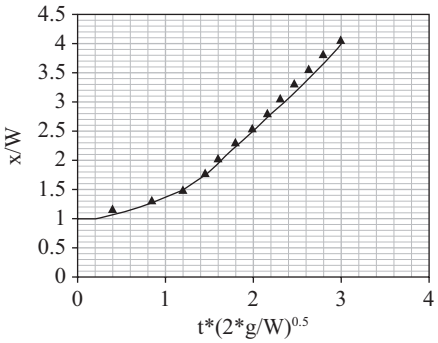

Fig. 4. Position of the leading edge *vs.* time; Experimental results: triangle symbol (▲); Present work: solid line (—). (x is the horizontal position of the water leading edge, W is the width of the water column, g is the gravity acceleration, and t is the simulation time.)

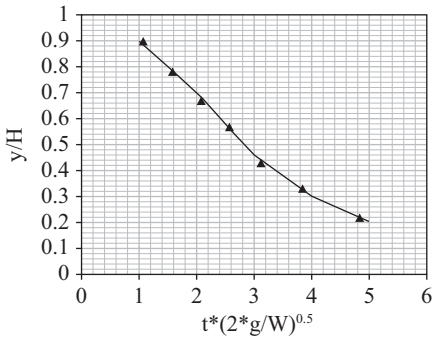

Fig. 5. Maximum column height *vs.* time; Experimental results: triangle symbol (▲); Present work: solid line (—).

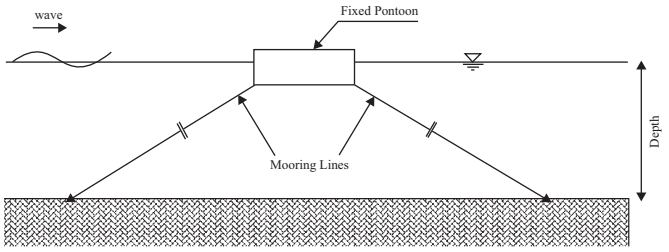

Fig. 6. Schematic of the problem.

between the design parameters. Fig. 6 illustrates the considered structures. As shown in the figure, the structures are completely moored and under the effect of the wave load.

In order to investigate how the selection of the cylinder geometry affects the hydrodynamic coefficients, a cylinder with four different cross sections is considered. Table 1 shows the geometry of pontoons.

For modeling the waves and in order to investigate the effect of different Reynolds numbers, four waves have been chosen. Reynolds number can be defined for a number of different situations where a fluid is in motion relative to a surface. These definitions generally include the fluid properties of density and viscosity, plus a velocity and a characteristic

Table 1. Illustration of Four different geometries.

Geometry	
Rectangular cylinder (H*L) Rec1	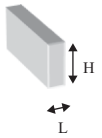
Rectangular cylinder (H*2L) Rec2	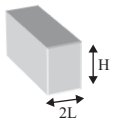
Rectangular cylinder (H*3L = H*H) Rec3	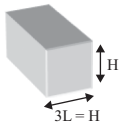
Circular Cylinder	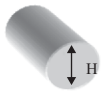

length or characteristic dimension. This dimension is a matter of convention - for example a radius or diameter is equally valid for spheres or circles, but one is chosen by convention. The general form of the Reynolds number is as follows:

$$\mathrm{Re} = \frac{\rho V L}{\mu} = \frac{V_{\max} L}{\nu} \tag{4}$$

where $V_{\max}$ [m/s] is the Maximum wave particle velocity at the crest of wave, L [m] is a characteristic linear dimension, μ is the dynamic viscosity of the fluid, ν is the kinematic viscosity ($\nu = \mu/\rho$) (m^2/s), ρ is the density of the fluid (kg/m^3) [12].

Another important property for choosing these waves is the water depth in which such waves could physically be possible. Based on the classification done by Dean and Dalrymple (2000) [7], when depth to wavelength ratio (i.e. h/L) is < 1/20, then the structure is assumed to encounter shallow water waves (i.e. long waves), and if 1/20 < h/L < 1/2, the structure is assumed to encounter intermediate depth waves and when h/L > 1/2, the structure is assumed to encounter deep water waves (i.e. short waves). It may be noted that, due to this dimensionless representation, a 200 m long wave in 1000 m of water has the same relative depth as a 0.2 m wave in 1 m of water. It is important to assess different cross sections of pontoons at different depths. Therefore, the waves have been selected in a way that the analysis would correspond to a wide range of depths from deep to shallow waters. Table 2 shows the wave characteristics and Table 3 illustrates its corresponding Reynolds numbers.

V. MESH STUDY

In order to obtain reliable results, it is important to use suitable mesh element size for the domain discretization.

Table 2. Wave parameters and depth classification.

Wave parameters	W1	W2	W3	W4
Height (m)	0.5	0.5	0.5	0.5
Depth (m)	8	6	4	2
ω (1/s)	0.7	0.5	0.3	0.1
Period (s)	1.42	2	3.33	10
Wave Length (m)	3.14822	6.24516	15.90455	43.699
Maximum Particle Velocity (m/s)	1.8205	1.0094	0.5624	0.2552
H/L	2.51 >> 1/2	0.96 > 1/2	0.25 >> 1/20	0.046 < 1/20
Depth Classification	Deep Water	Deep Water (near Intermediate)	Intermediate Water	Shallow Water

Table 3. Reynolds numbers in various wave parameters and geometries.

Geometry	Wave type	Reynolds Number
Rec1	W1	1.8205×10^6
	W2	1.0094×10^6
	W3	0.5624×10^6
	W4	0.2552×10^6
Rec2	W1	3.641×10^6
	W2	2.0188×10^6
	W3	1.1248×10^6
	W4	0.5104×10^6
Rec3	W1	5.4615×10^6
	W2	3.0282×10^6
	W3	1.6872×10^6
	W4	0.7656×10^6
Circular Cylinder	W1	5.4615×10^6
	W2	3.0282×10^6
	W3	1.6872×10^6
	W4	0.7656×10^6

Therefore, in this section, different element sizes ranging from 25 mm to 150 mm, are applied to one of the above mentioned cases (pontoon R2 and wave W3) to find a reliable mesh size. In Fig. 7, generated mesh for each mesh size is illustrated.

Drag force exerted on the pontoon versus mesh element size is plotted in Fig. 8. The drag force is calculated for the moment when the wave crest reaches the pontoon.

As shown in Fig. 8, the result converges to a specific drag, as the mesh size is reduced to 25 mm and the calculated value of the drag hardly changes from an element size of 50 mm to 25 mm. Therefore, an element size of 50 mm is adopted for the rest of the calculations.

VI. RESULTS AND DISCUSSIONS

Based on the computer code developed for modeling the outlined problem, lift and drag as well as the transmission coefficient have been calculated for different Reynolds number and geometric profiles.

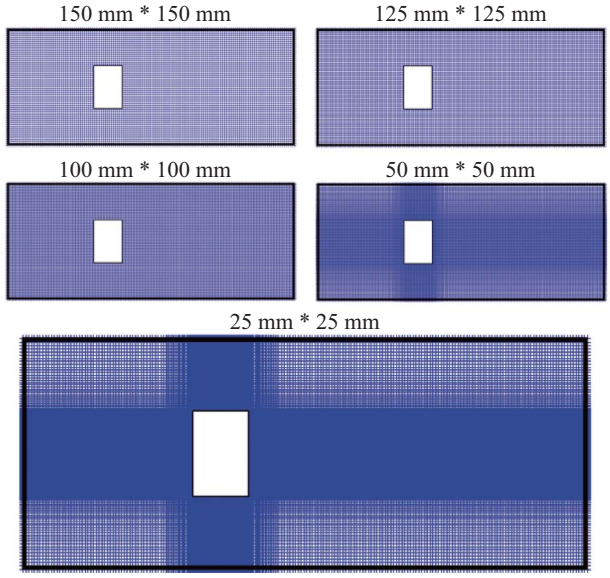

Fig. 7. Generated mesh for different mesh sizes.

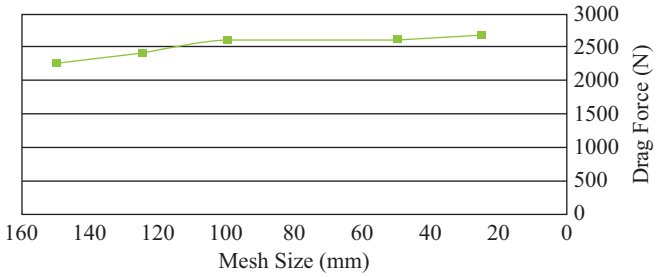

Fig. 8. Drag force *vs.* mesh element size.

Eq. (5) shows the relationship between the lift and drag forces and their coefficients.

$$C_D = \frac{Drag\ \ Force}{\frac{1}{2}\rho V^2 A}$$

$$C_L = \frac{Lift\ \ Force}{\frac{1}{2}\rho V^2 A} \tag{5}$$

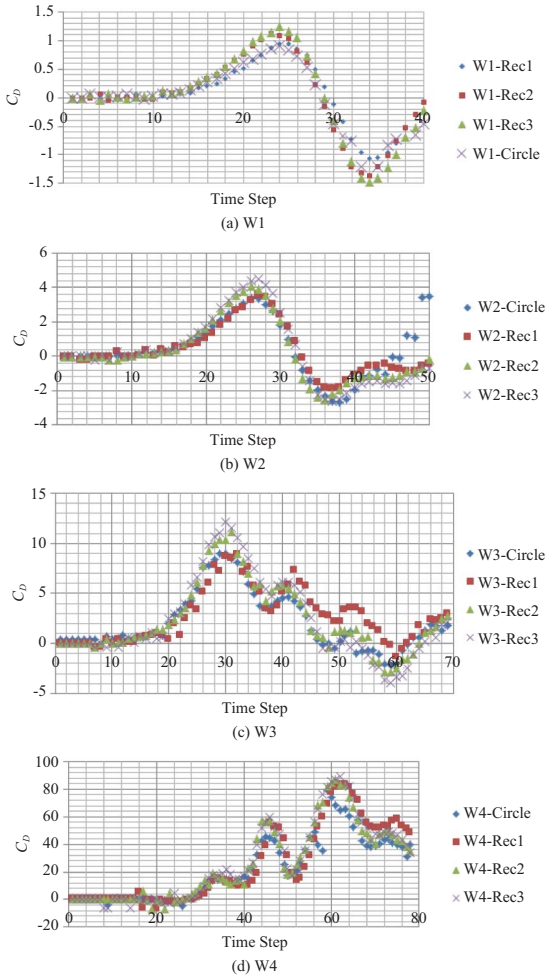

Fig. 9. Drag coefficient (C_D) for different geometries under wave (a) W1 (b) W2 (c) W3, and (d) W4.

where ρ is the water density, V is the fluid velocity and A is the projected area. The transmission coefficient is given by

$$C_T = \frac{H_T}{H_I}, \tag{6}$$

where H_T is the transmitted height while H_I is the incident wave height.

Calculated drag and lift coefficients are shown in Figs. 9 and 10. Fig. 9 illustrates the drag coefficient for four different geometries under W1 wave load. Each time step is considered to be 0.2 seconds.

Table 4 illustrates the maximum drag coefficient of different pontoon cross sections under different waves. As evidenced in Fig. 9 and Table 4, the drag coefficient for the rectangular cross section 3 (Rec3) is the highest while the drag coefficient for the circular cross section (Circle) is the lowest. This can be attributed to the perpendicular face of the rectangular cross section against the wave. In fact, in wave-structure interaction, rectangular structure unlike the circular

Table 4. CDmax for different pontoon cross sections in different waves.

		Circle	Rec1	Rec2	Rec3
W1	Deep	0.8921	0.9483	1.1341	1.2348
W2	Deep	3.32037	3.5859	4.054	4.4952
W3	Intermediate	8.997	8.66	11.1	12.1
W4	Shallow	79.17	82.88	86.94	89.21

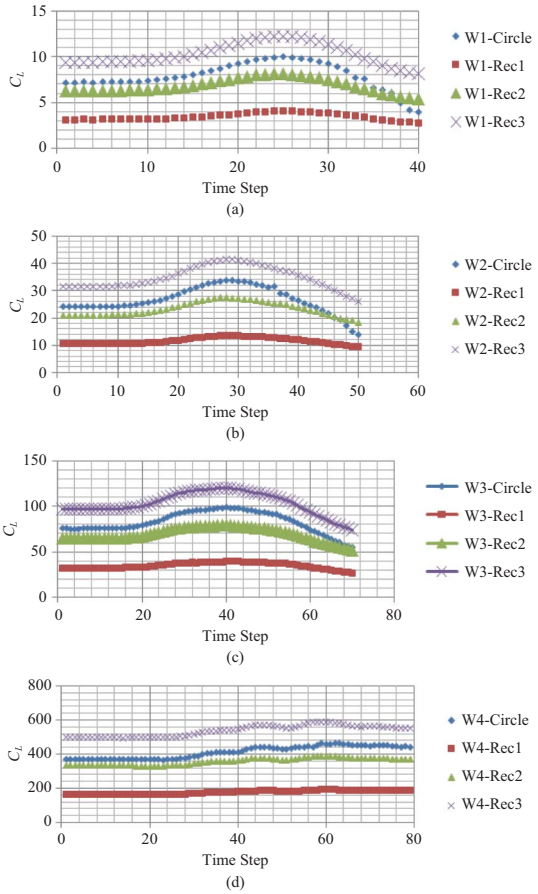

Fig. 10. Lift coefficient (C_L) for different geometries under waves (a) W1 (b) W2 (c) W3, and (d) W4.

structure, does not allow the water to slip over the cylinder (the curvature of the circle reduces the wave impact pressure and it allows the water to slip over it). Therefore, the wave momentum is largely transmitted to the rectangular cylinder and that indeed causes the drag coefficient of the rectangular structure to be more than that of the structure with circular cross section. Surprisingly, the Drag coefficient for Rec1 is almost the same as the Drag coefficient for the Circle. Once again, looking at their dimensions and geometries, it is concluded that a circular structure with diameter D = H, has approximately a drag coefficient equal to that of a rectangular structure with the same height, H, but with a width of H/3.

Among the three different rectangular cross sections, Rectangle 3 has the highest value of the drag coefficient. This

Table 5. CLmax for different pontoon cross sections in different waves.

		Circle	Rec1	Rec2	Rec3
W1	Deep	9.95	4.03	8.12	12.24
W2	Deep	33.67	13.48	27.41	41.42
W3	Intermediate	98.65	38.98	79.26	119.99
W4	Shallow	463.25	198.31	385.47	589.43

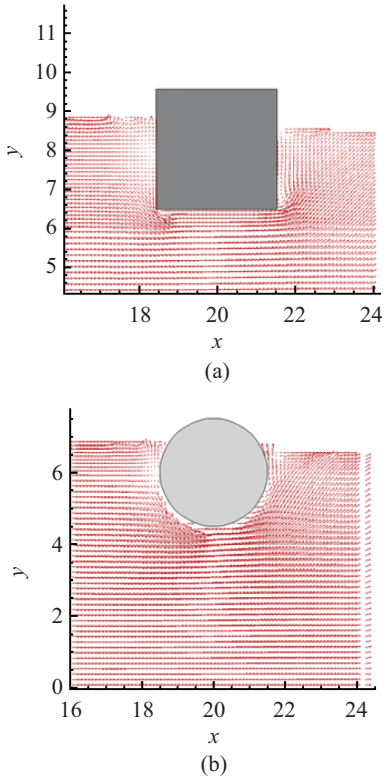

Fig. 11. Velocity vector fields at maximum drag condition for (a) Rectangular and (b) Circular cross sections.

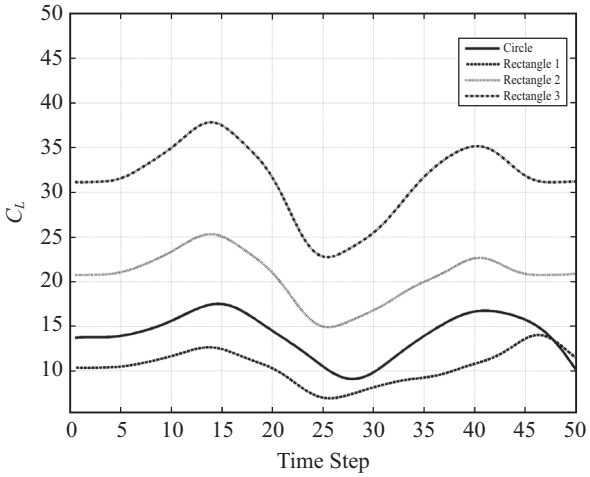

Fig. 12. Lift coefficient (C_L) in deep water for Rectangles 1, 2, 3 and for the circular cross section.

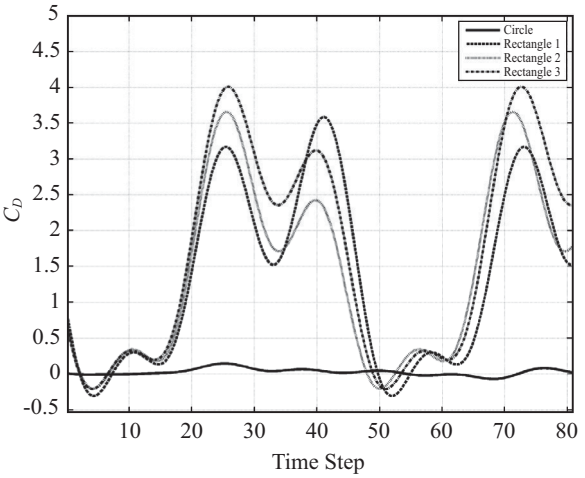

Fig. 13. Drag coefficients (C_D) in intermediate water for Rectangles 1, 2, 3 and for the circular cross section.

can be explained by the fact that the friction drag of the bottom of the cylinder increases with width. Friction drag is related to the tangential component of the drag. As evidenced in Fig. 9, the friction drag has the most influence on Rectangle 3 which has the largest width.

Plots of velocity vector fields at a time step where the rectangular (Rectangle 3) and circular pontoons exhibit the maximum drag are presented in Fig. 11.

The maximum lift coefficients of different pontoon cross sections under different waves are shown in Table 5. The analyses reveal that the most important factor affecting the lift force is the buoyancy force of the structure. As a matter of fact, the rates of increase or decrease of the lift coefficient depend on the area of the cross section surface of the structure in the water, due to the presence of the wave. Fig. 12 illustrates the lift coefficients for different pontoon structures.

In the intermediate water, due to the changes in wave parameter, the shapes of the drag coefficients are different. Here, the three rectangular cross sections display similar behavior. Rectangle 3 has the highest value among others. Surprisingly, as shown in Fig. 13, the drag coefficient of the circular case which was supposed to be small compared to the rectangular cases is shown to be much lower than the expected value.

Comparison of the drag coefficients for the deep and intermediate waters indicate that, at the same wave height, the maximum drag coefficient exhibited by Rectangle 3 structure in the case of deep water is 7.5, while it decreases to 4.2 in the case of intermediate water.

Fig. 14 illustrates the lift coefficients of different cross sections in intermediate water. Again, it seems that the buoyancy forces have the highest effect on the lift coefficient.

For clear demonstration of the discrepancies among the calculated drag and lift coefficients for the rectangular cases of

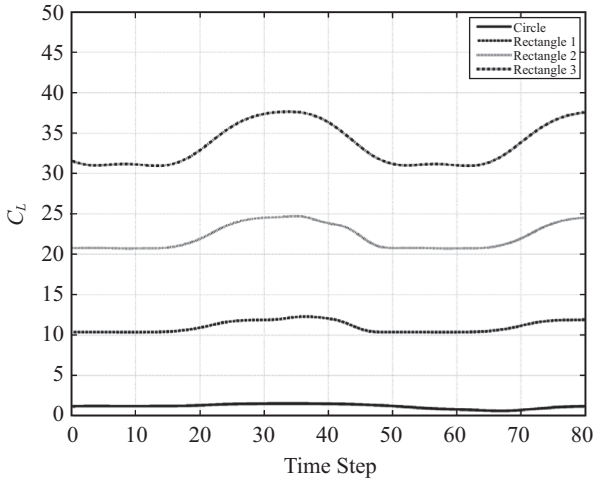

Fig. 14. Lift coefficients (C_L) in intermediate water for Rectangles 1, 2, 3 and for the circular cross section.

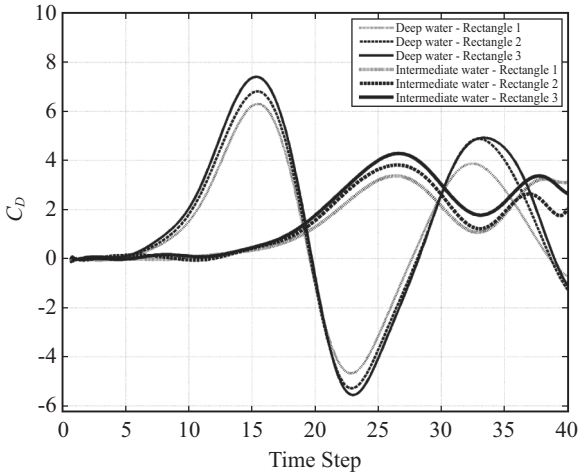

Fig. 15. Comparison of Drag coefficients (C_D) in deep and intermediate water for Rectangles 1, 2 and 3.

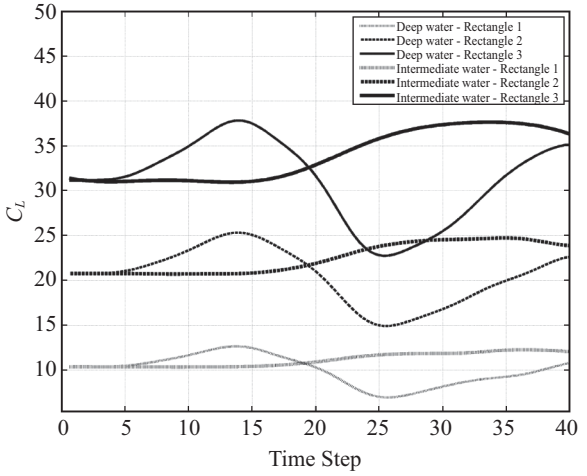

Fig. 16. Comparison of Lift coefficients (C_L) in deep and intermediate water for Rectangles 1, 2, and 3.

deep and intermediate waters, all plots are assembled in Figs. 15 and 16. Fig. 15 shows the plots of drag coefficients, while Fig.16 demonstrates the plots of lift coefficients.

It can be deduced from these figures that the maximum drag exhibited by these structures in intermediate water must be less than those in deep water. Therefore, one can easily conclude that the wave load on a rectangular pontoon structure in deep water is a strong influential factor in design considerations.

On the other hand, the drag coefficient of the circular cross section was shown earlier to be less than those with rectangular sections. This shows the lesser impact of the circular cylinder on the waves.

Finally, to assess the efficacy of each shape on the wave parameters, the important parameter which should be analyzed is the transmission coefficient. Fig. 17 illustrates the water elevation before and after the pontoon during the time of passage of the wave. The waves illustrated here are measured 5 cm before and 5 cm after the pontoon. This is why the reflection of the wave can be seen in the water level before the pontoon.

Hydrodynamic behaviors of the pontoons with different cross sections are well illustrated in Figs. 18 and 19, where the transmission coefficients of all the above cases are assembled together. The variation of the transmission coefficient of each pontoon is shown in different waves in Fig. 18. It can be concluded from the plots of Fig. 18 that the circular case has approximately 7% higher transmission coefficient than others in average under all waves except for the wave number 4 which represents the lowest Reynolds number for all geometries. This can be clearly seen in Fig. 19 which illustrates the transmission coefficients versus the Reynolds number.

The transmission coefficients of different cases are shown in Table 6.

It seems that at low Reynolds numbers, the influence of the cross section of the pontoon on the value of K_t decreases. Accordingly, K_t stays approximately the same for all cross sections for W4.

VII. CONCLUSION

A numerical investigation was performed to identify a simple, inexpensive and effective type of fixed pontoon under regular waves. Four different types of pontoons were considered in this study; three with quadrilateral cross sections and one with circular cross section. In order to investigate the flow field, Navier-Stokes as well as volume of fluid equations were solved using finite volume and volume of fluid methods. Four regular waves in deep, intermediate and shallow waters were chosen and the fixed structures were studied under these wave loads. The pontoons were considered moored such that all degrees of freedom were restrained and the hydrodynamic coefficients for each pontoon were calculated.

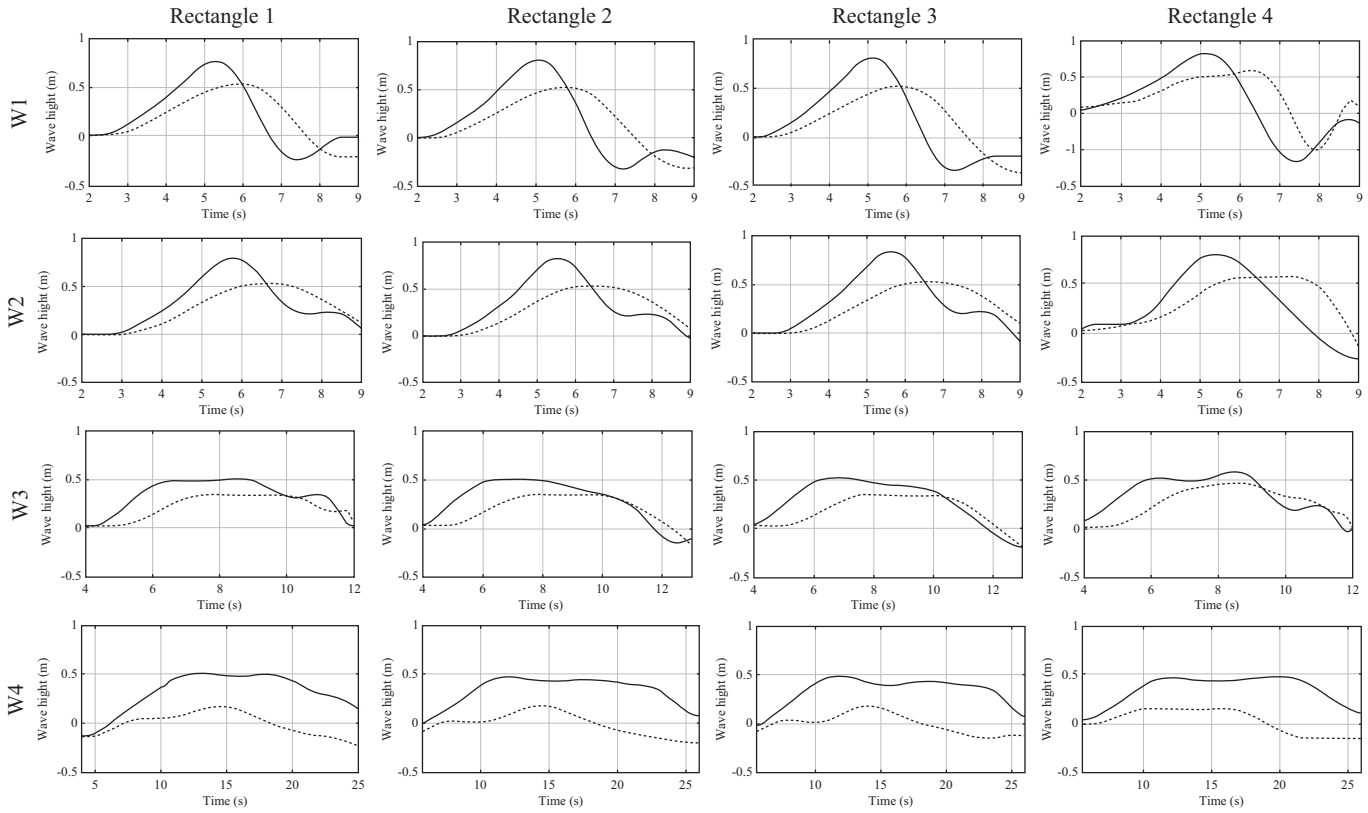

Fig. 17. Water level before (—) and after (-----) the pontoon in different cases.

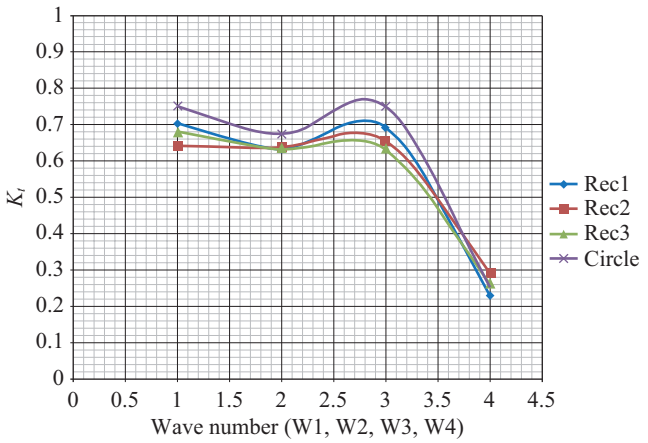

Fig. 18. Transmission coefficients (K_t) for all cross sections in different waves.

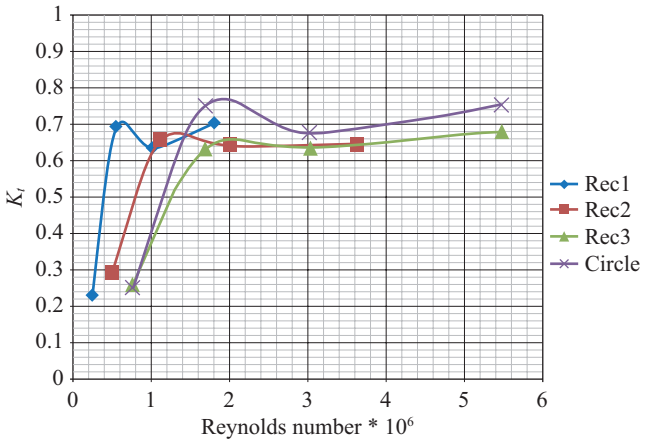

Fig. 19. Transmission coefficients (K_t) for all pontoon cross sections at different Reynolds numbers.

Computed results indicate that the drag coefficient in structures with circular cross section was approximately 33% less than the drag coefficient of the largest rectangular cross section (Rec3). Furthermore, comparison of the results for three different quadrilateral sections showed that, by increasing the width of the rectangular pontoon, while keeping its height fixed, the drag coefficient increased. These studies further indicate that the lift coefficient is under the full effect of buoyancy phenomenon. Investigation of the transmission coefficients was also conducted and results showed that, increasing the depth in the case of circular cross section would cause an increase in the transmission coefficient. However, in the case of rectangular cross sections, increasing the width of the pontoon would cause a decrease in the transmission coefficient in all waves.

The transmission coefficients for various geometries under different waves were calculated. Based on the findings, it was deduced that the transmission coefficient at lower

Table 6. K_t for different pontoon cross sections in different waves.

		Circle	Rec1	Rec2	Rec3
W1	Deep	0.75	0.7	0.64	0.68
W2	Deep	0.68	0.64	0.64	0.64
W3	Intermediate	0.75	0.69	0.65	0.63
W4	Shallow	0.25	0.23	0.29	0.26

Reynolds numbers (less than 10^6) was not severely affected by the cross section of the pontoon. However, at higher Reynolds numbers (more than 10^6), the transmission coefficient was 7% higher for the circular section.

In summary, one can conclude that the rectangular cross sections are more capable to absorb the wave momentum and in particular those with larger width are most appropriate for breakwater applications. On the other hand, the curvature of circular cylinders allows the wave pass without significant energy absorption, especially in the intermediate waters which makes the curved sections more suitable for structures (like fixed bridges or dikes) over which the wave is needed to pass with a minimum effect.

REFERENCES

1. Bayram, A., "Experimental study of a sloping float breakwater," *Ocean Engineering*, Vol. 27, pp. 445-453 (2000).
2. Bhatta, D. D. and Rahman, M., "Computational methods and experimental measurements to a floating cylinder in waves," *Proceedings of the Computational Modeling of Free and Moving Boundary Problems*, pp. 395-402 (1993).
3. Bonet, J. and Lok, T.-S., "Variational and momentum preservation aspects of Smooth Particle Hydrodynamics," *Computer Methods in Applied Mechanics and Engineering*, Vol. 180, pp. 97-115 (1999).
4. Braza, M., Chassaing, P., and Minh, H. H., "The numerical study and physical analysis of the pressure and velocity fields in the near wake of a circular cylinder," *Journal of Fluid Mechanics*, Vol. 165, pp. 79-130 (1986).
5. Chaplin, J. R., "On the irrotational flow around a horizontal cylinder beneath waves," *Journal of Applied Mechanics*, Vol. 48, pp. 689-694 (1981).
6. Chaplin, J. R., "Orbital flow around a circular cylinder Part 2 Attached flow at larger amplitudes," *Journal of Fluid Mechanics*, Vol. 246, pp. 397-418 (1993).
7. Dean, R. G. and Dalrymple, R. A., *Water Wave Mechanics for Engineers and Scientists*, World Scientific Publishing (2000).
8. Drimer, N., Agnon, Y., and Stiassnie, M., "A simplified analytical model for a floating breakwater in water of finite depth," *Applied Ocean Research*, Vol. 14, pp. 33-41 (1992).
9. Ghia, U., Ghia, K. N., and Shin, C. T., "High-Re solutions for incompressibe flow using the Navier-Stokes equations and a multigrid method," *Journal of Computational Physics*, Vol. 48, pp. 387-411 (1982).
10. Hwang, C. and Tang, F. L. W., "Studies on rectangular surface barrier against short waves," *Proceedings of the 20th International Conference of Coastal Engineering ASCE*, pp. 1915-1928 (1986).
11. Isaacson, M. and Bhat, S., "Wave propagation past a pile-restrained floating breakwater," *International Journal of Offshore Polar Engineering*, Vol. 8, pp. 265-269 (1998).
12. Jung, K. H., Chang, K.-An, and Huang, E. T., "Two dimensional flow characteristics of wave Interactions with a fixed rectangular structure," *Ocean Engineering*, Vol. 31, pp. 975-998 (2004).
13. Kriezi, E. E., Karambas, Th. V., Prinos, P., and Koutitas, C., "Interaction of floating breakwaters with waves in shallow waters," *Proceedings of the 29th International Association for Hydro-Environment Engineering and Research (IAHR) Conference*, Bejing, China (2001).
14. Liang, N. K., Huang, J. S., and Li, C. F., "A study of buoy floating breakwater," *Ocean Engineering*, Vol. 31, pp. 43-60 (2004).
15. Lin, P., "Review of numerical modeling of water waves," *Journal of Waterway, Port, Coastal, and Ocean Engineering*, Vol. 136, pp. 125-126 (2010).
16. Mader, C. L., *Numerical Modeling of Water Waves*, 2nd Edition, CRC Press (2004).
17. Mani, J. S., "Design of Y-frame floating breakwater," *Journal of Waterway, Port, Coastal, and Ocean Engineering*, ASCE, Vol. 117, pp. 105-119 (1991).
18. McCartney, B. L., "Floating breakwater design," *Journal of Waterway, Port, Coastal, and Ocean Engineering*, ASCE, Vol. 3, pp. 304-318 (1985).
19. Murani, K. and Mani, J. S., "Performance of cage floating breakwater," *Journal of Waterway, Port, Coastal, and Ocean Engineering*, ASCE, Vol. 123, pp. 172-179 (1997).
20. Sannasiraj, S. A., Sundar, V., and Sundaravadivelu, R., "Mooring forces and motion responses of pontoon-type floating breakwaters," *Ocean Engineering*, Vol. 25, pp. 27-48 (1997).
21. Sarpkaya, T., "Computational methods with vortices - The 1988 Freeman scholar lecture," *Journal of Fluid Engineering*, Vol. 111, pp. 5-52 (1989).
22. Tseng, M. H., "Kinematic wave computation using an efficient implicit method," *Journal of Hydroinformatics*, Vol. 12, pp. 329-338 (2010).
23. Ubbink, O., *Numerical Prediction of Two Fluid Systems with Sharp Interface*, Ph.D. Thesis, University of London (1997).
24. Williams, A. N. and McDougal, W. G., "Flexible floating breakwater," *Journal of Waterway, Port, Coastal, and Ocean Engineering*, ASCE, Vol. 117, pp. 429-450 (1991).
25. Williams, A. N. and Abul-Azm, A. G., "Dual pontoon floating breakwater," *Ocean Engineering*, Vol. 24, pp. 465-478 (1997).
26. Williams, A. N., Lee, H. S., and Huang, Z., "Floating pontoon breakwater," *Ocean Engineering*, Vol. 27, pp. 221-240 (2000).
27. Zhang, J. and Mercier, R., "Foreword," *Ocean Engineering*, Vol. 32, pp. 765-766 (2005).